

Electron-Donor Engineering of Heptazine-Based Donor-Acceptor Conjugated Microporous Polymers for Efficient Metal-Free Photocatalytic Hydrogen Evolution

*Lin-Fang Yang,^a Yi-Zhou Zhu,^{*a} Cheng-Cheng Zhang,^a and Jian-Yu Zheng^{*a}*

^a State Key Laboratory and Institute of Elemento-Organic Chemistry, College of Chemistry, Nankai University, 94 Weijin Road, Tianjin, 300071, China

E-mail: zhuyizhou@nankai.edu.cn (Yi-Zhou Zhu); jyzheng@nankai.edu.cn (Jian-Yu Zheng)

CONTENS

1. Experimental Section	3
2. Synthetic Procedure	8
3. Characterization	11
4. PHE Performance	15
6. Dynamics Behaviours of Photoexcited Carriers	22
7. Theoretical Calculations	25
8. NMR Spectra	28
References	31

1. Experimental Section

1.1. Reagents

All reagents were used as received unless otherwise noted. 5,5-dimethyl-1-pyrroline *N*-oxide, 2,2,6,6-tetramethylpiperidiny-1-oxide, melamine, phosphorus oxychloride, phosphorus pentachloride, pyrene, nitrobenzene, potassium carbonate, sodium carbonate, bis(triphenylphosphine)palladium dichloride, ethanol, 4-aminophenylboronic acid picol ester, tetrakis(triphenylphosphine)palladium, triphenylphosphine, 1,4-dioxane and *N,N*-diisopropylethylamine were purchased from Anhui Zesheng Technology Co., Ltd.

1.2. Materials Characterization

Solution-state ^1H NMR and ^{13}C NMR spectroscopies were recorded on a 400 MHz spectrometer (Bruker Ascend 400 Spectrometer) with tetramethylsilane ($\delta = 0$) as internal standard. Solid-state ^{13}C cross polarization magic angle spinning NMR spectroscopies (CP-MAS NMR) were performed by VANCE NEO 400 spectrometer, equipped with a 9.4 T magnet. Fourier transform infrared spectra (FT-IR) were recorded on a Thermofisher Scientific Nicolet iS50 spectrometer between 4000-400 cm^{-1} . Powder X-ray diffraction (PXRD) patterns were obtained on a Japan Rigaku SmartLab diffractometer. X-ray photoelectron spectroscopies (XPS) were performed on an Axis Ultra DLD spectrometer, equipped with a prereduction chamber. Scanning electron microscopy (SEM) was measured on a FEI Apreo S LoVac microscope. Transmission electron microscopy (TEM) was performed on Tecnai G2 F20. Nitrogen adsorption-desorption isotherms were obtained on a nitrogen adsorption apparatus (Surface Area and Pore Analyzer Micromeritics ASAP 2460) with all samples degassed at 373 K for 12 h prior to measurements. Confocal laser scanning microscopy (CLSM) was measured on TCS SP5.

The steady-state photoluminescence (PL) and temperature-dependent PL spectra from 180 K to 300 K were collected by a HITACHI F-4600 spectrofluorometer. The UV-Vis absorption spectra were recorded on a UV-2600 spectrophotometer (Shimadzu, Japan), equipped with an integrating sphere assembly and BaSO_4 was used as reflectance sample. The optical bandgap (E_g) was calculated according to following equation: $(\alpha h\nu)^{1/n} = B(h\nu - E_g)$, where α is the adsorption coefficient, h is the Planck constant, ν is the light frequency, B is a constant and E_g is the corresponding bandgap. In addition, the n factor is determined by the nature of the electron transition. Particularly, $n = 1/2$ means a direct bandgap transition, and $n = 2$ suggests an indirect

bandgap transition. In this work, the value of n for all polymers equals 1/2 because of its direct transition nature.

Femtosecond transient absorption spectrometer consist of a regenerative amplified Ti: sapphire laser system (Coherent) and Helios pump-probe system S14 (Ultrafast Systems). The regenerative-amplified Ti: sapphire laser system (Legend Elite-1K-HE, center wavelength of 800 nm, pulse duration of 25 fs, pulse energy of 4 mJ, repetition rate of 1 kHz) was seeded with a mode-locked Ti: sapphire laser system (Vitara) and pumped with a Nd: YLF laser (Evolution 30). The output 800 nm fundamental of the amplifier was split into two beam pulses. The main part of the fundamental beam went through the optical parametric amplifiers (TOPAS-C), whose output light was set as the pump light with wavelength of 840 nm and chopped by a mechanical chopper operating at frequency of 500 Hz. A small part of the fundamental beam was introduced into the TA spectrometer in order to generate the probe light. After passing through a motorized optical delay line, the fundamental beam was focused on a sapphire crystal or YAG crystal, which was used to generate the white light continuum (WLC) probe pulses with wavelength of 430 to 820 nm. The optical path difference between the pump light and the probe light, which is controlled by the motorized optical delay-line, was used to monitor the transient states at different pump-probe delay. A reference beam was split from the WLC in order to correct the pulse-to-pulse fluctuation of the WLC. The pump was spatially and temporally overlapped with the probe beam on the sample. Excitation energy of the pump pulse was set to $2 \mu\text{J}/\text{cm}^2$ to avoid singlet-singlet annihilation.

1.3. Photocatalytic Hydrogen Evolution Measurements¹⁻⁷

Photocatalytic hydrogen evolution (PHE) measurements of all polymers were carried out on an automatic online gas analysis photocatalytic system (CEL-PAEM-D8-PLUS, Beijing China Education Au-light Co. Ltd., China) with a 300 W Xe lamp as the light source. Typically, the polymer was fully dispersed in a mixture of deionized water, co-solvent and sacrificial hole-scavenger (Detailed reaction conditions can be seen at **Table S1**). Then, the reaction flask was connected to the photocatalytic equipment. Before the photocatalytic reaction, the gas pressure in the photocatalytic system was decreased to minimum by degassing. Afterwards, the reaction mixture was illuminated by a 300 W Xenon lamp source (The actual radiant flux is 210 W) with stirring in negative pressure. Circulating cooling water was employed to keep the photocatalytic reaction temperature at 10 °C. The generated H₂ was collected and measured by a gas

chromatograph (GC7920) installed with a thermal conductive detector. Visible light ($\lambda > 420$ nm) was achieved by using a long pass cut-off filter.

The apparent quantum yields (AQY) measurement for hydrogen evolution was performed using 10 mg **Y4** and measured with monochromatic light obtained by using band pass. AQY for H₂ evolution at monochromatic light irradiation was estimated as below equation.

$$\eta = \frac{2 \times M \times N_A \times h \times c}{S \times P \times t \times \lambda}$$

M is the amount of hydrogen molecules (mol), N_A is Avogadro constant (6.022×10^{23} mol⁻¹), h is the Planck constant (6.626×10^{-34} J·s), c is the speed of light (3×10^8 m s⁻¹), S is the irradiation area (m²), P is the intensity of irradiation light (W m⁻²), t is the photoreaction time (s), λ is the wavelength of the monochromatic light (m).

1.4. Electrochemical Experiments

The photocurrent response experiments were performed on a Zennium electrochemical workstation (ZAHNER, Germany) with a standard three-electrode cell using Ag/AgCl electrode as the reference electrode, a Pt wire as the counter electrode, sample deposited indium tin oxide (ITO) glass plate as the working electrode, and 0.2 M Na₂SO₄ aqueous solution as the electrolyte solution. The working electrode was manufactured as follows: 5 mg catalyst was dispersed in a mixture solution of 300 uL ethanol and 20 uL Nafion. After sonicated for 30 min, the suspension was transferred onto an ITO conductive glass and dried in the air. The exposure area of the catalyst is 1 cm². The photocurrent density measurements were performed under visible light ($\lambda > 420$ nm, 20 W White light). The electrochemical impedance spectroscopy (EIS) and Mott-Schottky curves were measured on a CHI Instruments potentiostat/galvanostat (CHI660D) using a frequency ranged from 10⁶ Hz to 10⁻¹ Hz and 500, 1000 and 1500 Hz alternating current potential frequency, respectively.

1.5. Electron Paramagnetic Resonance (EPR) Measurements

Spin trapping-EPR and unpaired electrons-EPR measurements were recorded using a Bruker EPR spectrometer operating at the X-band frequency (9.85 GHz). For Spin trapping-EPR measurements, 5,5-dimethyl-1-pyrroline N-oxide (DMPO) and 2,2,6,6-tetramethylpiperidinyl-1-oxide (TEMPO) were used to detect superoxide anion radical (O₂^{-•}) and hole (h⁺). The detailed sample preparation were conducted as follows: catalysts (2 mg) were dispersed in a mixed solution of DMPO (20 uL/3

mL DMSO) or TEMPO (20 uL/3 mL H₂O). Before spin trapping-EPR tests, the mixture was stirred for 5 min under radiation with 20 W white light lamp ($\lambda > 420$ nm,) and then transported into quartz capillaries. For unpaired electrons-EPR measurements, catalyst (25 mg) was injected into nuclear magnetic tube without further treatment.

1.6. Theoretical Calculation^{8,9}

Theoretical calculations were carried out using the Gaussian 16 software package. All calculations were performed using the density functional theory (DFT) method. The geometries were optimized at the B3LYP-D3/6-311+G(d,p) level. The time-dependent DFT (TD-DFT) were calculated at the same level. The distribution of electrons and holes, heat map, inter-fragment charge transfer (IFCT), charge-transfer spectra (CTS) and density of states (DOS) were calculated by the Multiwfn 3.8 package using Hirshfeld atomic charge analysis. Besides Multiwfn, VMD was also used to draw the corresponding figures.

The distribution of electrons and holes were calculated by the following formula:

$$\begin{aligned}\rho^{hole}(r) &= \rho_{(loc)}^{hole}(r) + \rho_{(cross)}^{hole}(r) \\ \rho_{(loc)}^{hole}(r) &= \sum_{i \rightarrow a} (\omega_i^a)^2 \varphi_i \varphi_i - \sum_{i \leftarrow a} (\omega_i'^a)^2 \varphi_i \varphi_i \\ \rho_{(cross)}^{hole}(r) &= \sum_{i \rightarrow a} \sum_{j \neq i \rightarrow a} \omega_i^a \omega_j^b \varphi_i \varphi_j - \sum_{i \rightarrow a} \sum_{i \rightarrow b \neq a} \omega_i'^a \omega_j'^b \varphi_i \varphi_j \\ \rho^{ele}(r) &= \rho_{(loc)}^{ele}(r) + \rho_{(cross)}^{ele}(r) \\ \rho_{(loc)}^{ele}(r) &= \sum_{i \rightarrow a} (\omega_i^a)^2 \varphi_a \varphi_a - \sum_{i \leftarrow a} (\omega_i'^a)^2 \varphi_a \varphi_a \\ \rho_{(cross)}^{ele}(r) &= \sum_{i \rightarrow a} \sum_{i \rightarrow b \neq a} \omega_i^a \omega_i^b \varphi_a \varphi_b - \sum_{i \rightarrow a} \sum_{i \rightarrow b \neq a} \omega_i'^a \omega_i'^b \varphi_a \varphi_b\end{aligned}$$

Where ρ represents the density of electrons and holes, r is coordinate vector, φ is orbital wave function, i and j are the number of occupied orbital, a and b are the number of unoccupied orbital, $\sum_{i \rightarrow a}$ and $\sum_{i \leftarrow a}$ are the cycling of each excited state-de-excited state and ω' is the coefficient of excited configuration and de-excited configuration, respectively.

The hole and electron delocalization index (HDI and EDI) were calculated by the following formula:

$$HDI = 100 \times \sqrt{\int [\rho^{hole}(r)] dr}$$

6

$$EDI = 100 \times \sqrt{\int [\rho^{ele}(r)] dr}$$

The IFCT was calculated by the following formula:

$$\begin{aligned} Q_{R,S} &= \theta_{R,hole} \theta_{S,ele} \\ P_{S \rightarrow R} &= Q_{S,R} - Q_{R,S} \\ \Delta P_R &= \sum_{S \neq R} P_{S \rightarrow R} = \sum_{S \neq R} (Q_{S,R} - Q_{R,S}) \end{aligned}$$

Where $\theta_{R,hole}$ represents the number of electrons in R in the excited electrons, $\theta_{S,ele}$ is the number of electrons in S in the destination of electronic transfer. $Q_{R,S}$ is the number electron transfer from R to S, $P_{S \rightarrow R}$ is net number of electron transfer from S to R, ΔP_R is net charge number of electron in R.

The CTS was calculated by the following formula:

$$\begin{aligned} \varepsilon_{A,B}(E) &= \sum_i f_i Q_i^{A,B} G(E - E_i^{exc}) \\ \varepsilon_{A,A}(E) &= \sum_i f_i Q_i^{A,A} G(E - E_i^{exc}) \\ \varepsilon(E) &= \varepsilon_{A,A}(E) + \varepsilon_{A,B}(E) + \varepsilon_{B,A}(E) + \varepsilon_{B,B}(E) \end{aligned}$$

Where ε represents molar absorption coefficient, $\varepsilon_{A,B}$ is molar absorption coefficient caused by electron transfer from A to B, $\varepsilon_{A,A}$ is molar absorption coefficient caused by locally excited electrons in A, i is the cycling of each excited state, f is the oscillator strength, E is absorption wavelength, E^{exc} is stimulating energy, G is broadening function.

The total density of states (TDOS) and partial density of states (PDOS) were calculated by the following formula:

$$\begin{aligned} TDOS(E) &= \sum_i \delta(E - \varepsilon_i) \\ PDOS_A(E) &= \sum_i \theta_{A,i} F(E - \varepsilon_i) \end{aligned}$$

where DOS (E) represents the number of states within per unit energy interval at the position of energy (E), δ is dirac function, ε is orbital energy, θ is orbital composition, and F is broadening function.

The HER process involves two one-electron pathways, proton/electron transfer step and hydrogen release step:

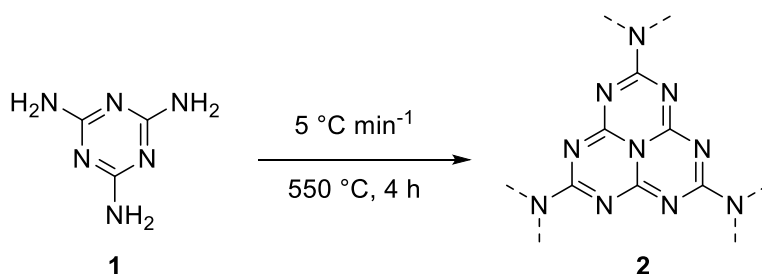


where * denotes the adsorption site and H* denotes the adsorbed H atom.

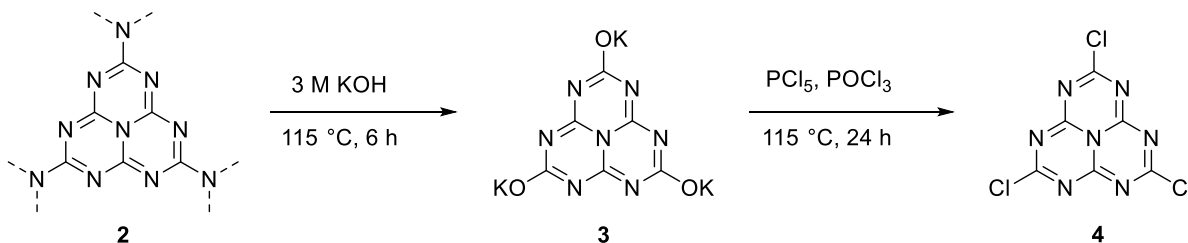
The Gibbs free energies were calculated at the B3LYP-D3/6-31G level by the following formula:

$$\Delta G = G(*\text{H}) - G(*) - 1/2G(\text{H}_2)$$

2. Synthetic Procedure



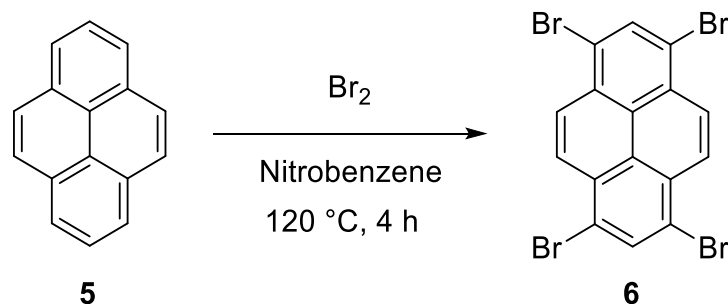
Synthesis of g-C₃N₄ (2).¹⁰ Melamine (40.0 g, 317.2 mmol) was placed in a ceramic crucible and heated to 550 °C at a rate of 5 °C min⁻¹ in a muffle furnace and stood for 4 h. After completed, the system was cooled to room temperature at an unrestricted rate and then the solid was ground to obtain compound **2** as a yellow powder.



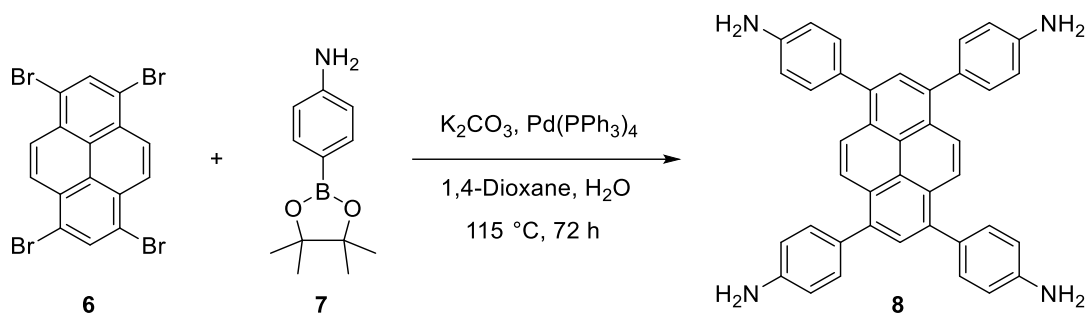
Synthesis of cyameluric chloride (4).¹¹ Compound **2** (10 g) was dispersed in a aqueous solution of KOH (3 M, 150 mL) and then the mixture was heated at 115 °C for 6 h. The solution was filtered while hot and the filtrate was cooled in an ice-water bath. After that, the precipitated white crystals were collected by filtration and washed with ice ethanol. Finally, the products were dried in a vacuum oven at 80 °C for 24 h without further treatment.

Compound **3** (6 g, 17.9 mmol) and PCl₅ (12 g, 57.7 mmol) were dispersed in POCl₃ (120 mL) at argon atmosphere. The mixture was heated at 115 °C for 24 h. After completed, the mixture was filtered and the filtrate was removed by rotary evaporator. The residue was further treated by Soxhlet extraction with toluene for 24 h. Then, the solvent was removed by rotary evaporator and the residue dried under vacuum for 6 h, giving the final product **4** as a light-yellow solid (3.5 g,

72% yield). IR (KBr, cm^{-1}): 1643, 1608, 1502, 1451, 1377, 1302, 1199, 1095, 957, 831, 647, 452. ^{13}C NMR (100 MHz, benzene- d_6 , ppm): δ 175.3 (C-Cl), 155.4 (N-C=N). Solid-state ^{13}C NMR (400 MHz, ppm): δ 165.3 (C-Cl), 155.0 (N-C=N).



Synthesis of 1,3,6,8-tetrabromopyrene (6).⁷ To a solution of pyrene (5.056 g, 25 mmol) in nitrobenzene (30 mL) was added dropwise bromine (6.6 mL, 120 mmol) at room temperature. Then, the mixture was heated at 120 °C for 4 h. After that, the mixture was cooled to room temperature and was filtered. The residue was further washed with methanol (50 mL) and acetone (50 mL), giving the final product **6** as a pale yellow solid (11.6 g, 90% yield). Since the product was insoluble, it was used in the next reaction without characterization.



Synthesis of 1,3,6,8-tetrakis(4-aminophenyl)pyrene (8, TAPPy).¹² Compound **6** (2.5 g, 4.83 mmol), **7** (5.065 g, 23.14 mmol), K_2CO_3 (3.82 g, 27.69 mmol) and $\text{Pd}(\text{PPh}_3)_4$ (1.11 g, 0.97 mmol) were dispersed in a mixture solution of 1,4-dioxane (100 mL) and H_2O (18 mL) at argon atmosphere and then the mixture was heated at 115 °C for 72 h. After the mixture was cooled to room temperature, 60 mL H_2O was added and then was filtered. The residue was washed with H_2O and MeOH until the washings were clear. The solid was further crystallized from 1,4-dioxane and dried under high vacuum for 6 h, giving compound **8** as a light-yellow solid (2.83 g, 91%). ^1H NMR (400 MHz, $\text{DMSO}-d_6$, ppm): δ 5.32 (s, 8H), 6.76-6.78 (d, $J = 8$ Hz, 8H), 7.33-7.35 (d, $J = 8$ Hz, 8H), 7.78 (d, 2H), 8.12 (s, 4H). ^{13}C NMR (100 MHz, $\text{DMSO}-d_6$, ppm): δ 114.39, 124.88, 126.57, 127.16, 128.03, 131.51, 137.58, 148.67.

3. Characterization

3.1. Solid-state ^{13}C NMR Spectra

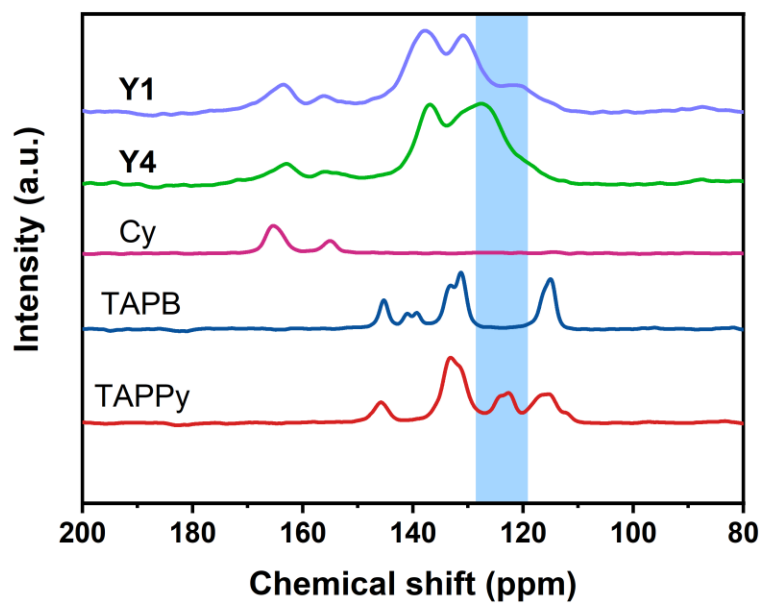


Fig. S1 Solid-state ^{13}C NMR spectra of **Y1**, **Y4** and their precursors.

3.2. Scanning Electron Microscope (SEM) Spectra

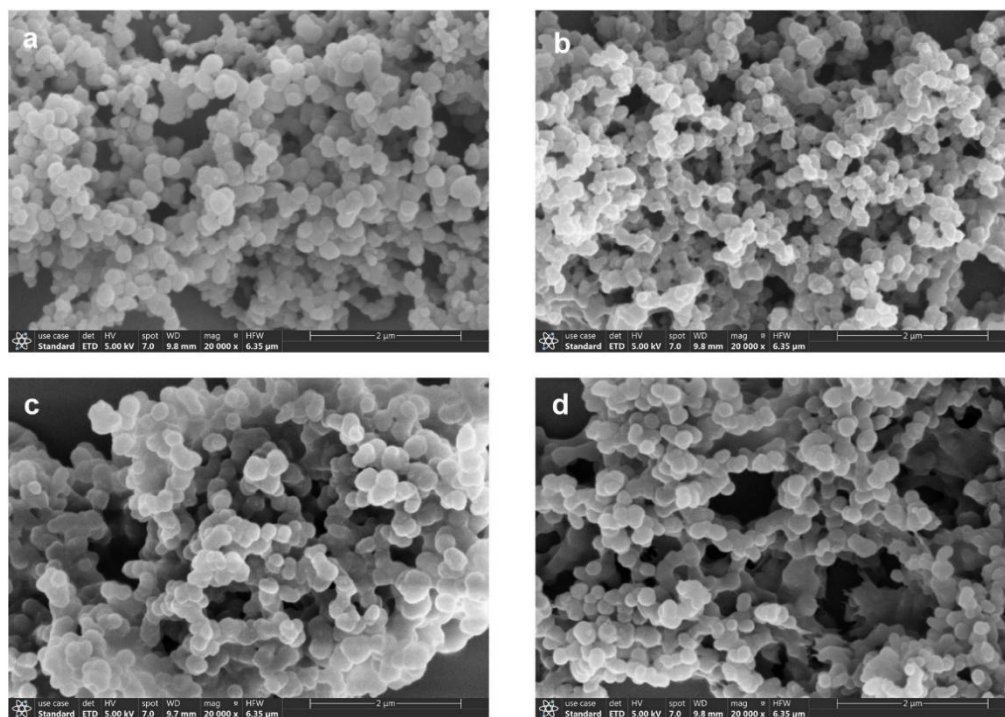


Fig. S2 SEM spectra of all polymers. (a) Y1; (b) Y2; (c) Y3; and (d) Y4.

3.3. Transmission Electron Microscopy (TEM) Spectra

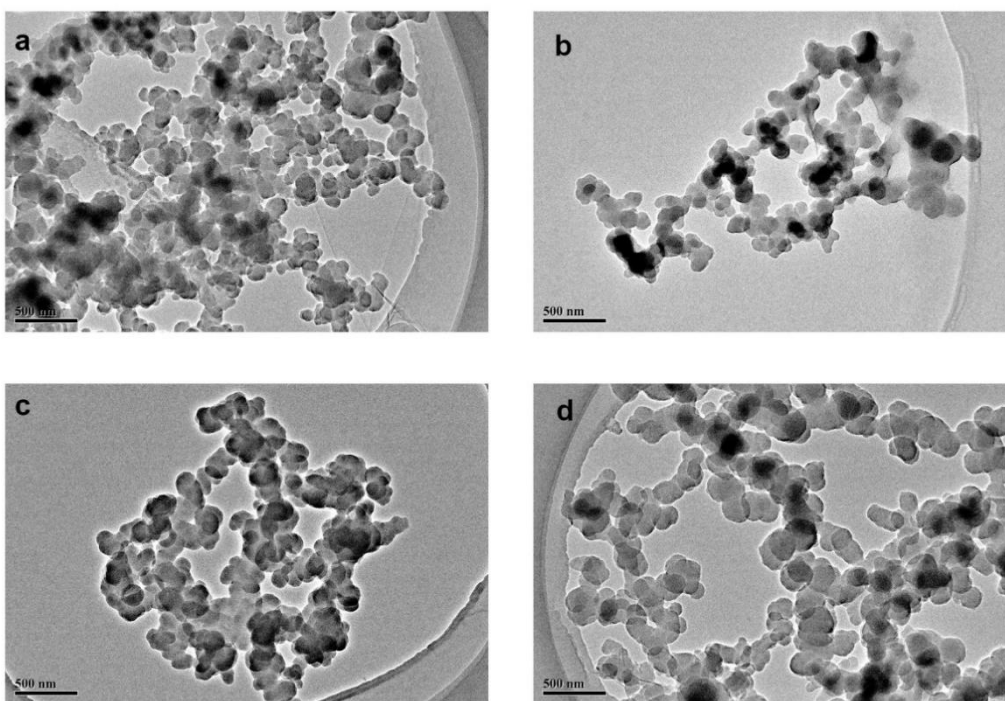


Fig. S3 TEM spectra of all polymers. (a) Y1; (b) Y2; (c) Y3; and (d) Y4.

3.4. Specific Surface Area and Porosity

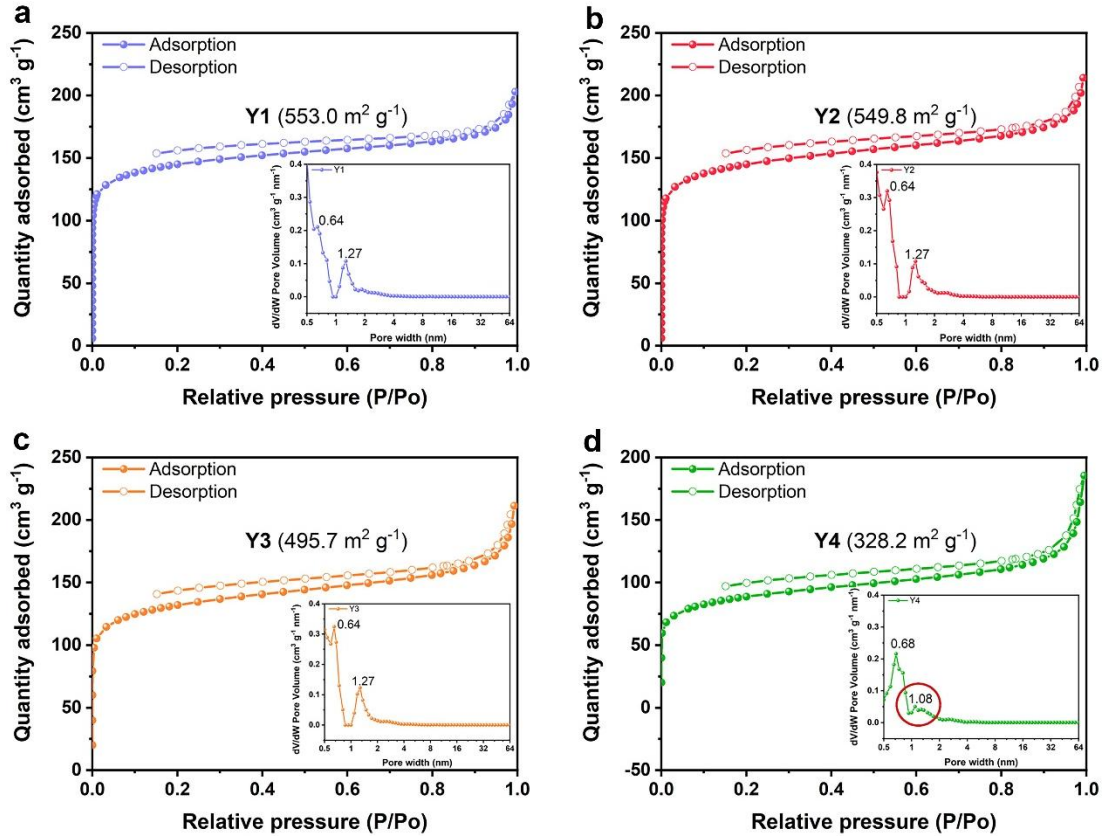


Fig. S4 N_2 adsorption-desorption isotherms. (a) Y1; (b) Y2; (c) Y3; and (d) Y4.

3.5. Optical Properties and Band Structures

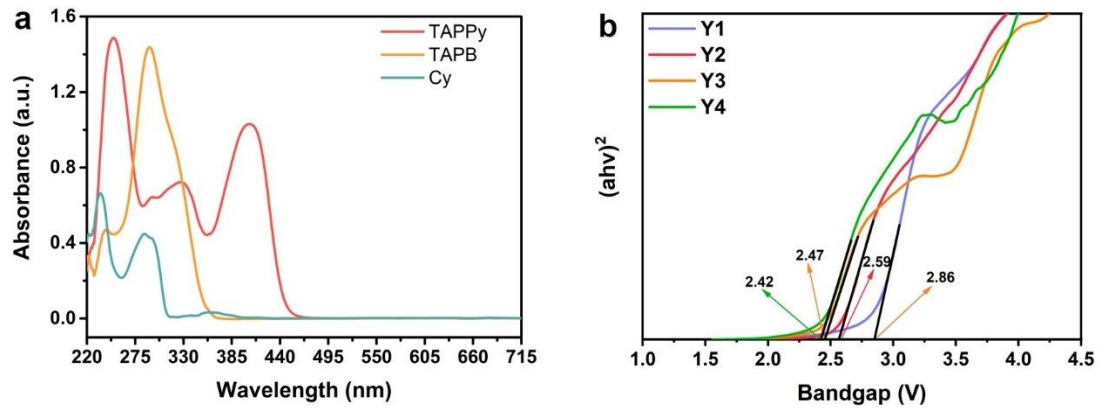


Fig. S5 (a) UV-vis absorption spectra of TAPPy, TPPB and Cy recorded in THF (10 μM). (b) Tauc plots spectra of all polymers.

3.6. Conduction Bands (CBs) Potentials

The positive slopes suggest all polymers are n-type semiconductors. Since the flat band potential lies 0.1 V lower than the CB for the n-type semiconductors, the conduction bands (CBs) potentials from **Y1** to **Y4** were calculated to be -1.64, -1.56, -1.53, -1.49 (V Vs. Ag/AgCl) according to the flat band potentials, respectively.¹⁵ The CBs potentials from **Y1** to **Y4** relative to NHE are further calculated to be -1.44, -1.36, -1.33, -1.29 (V Vs. NHE).

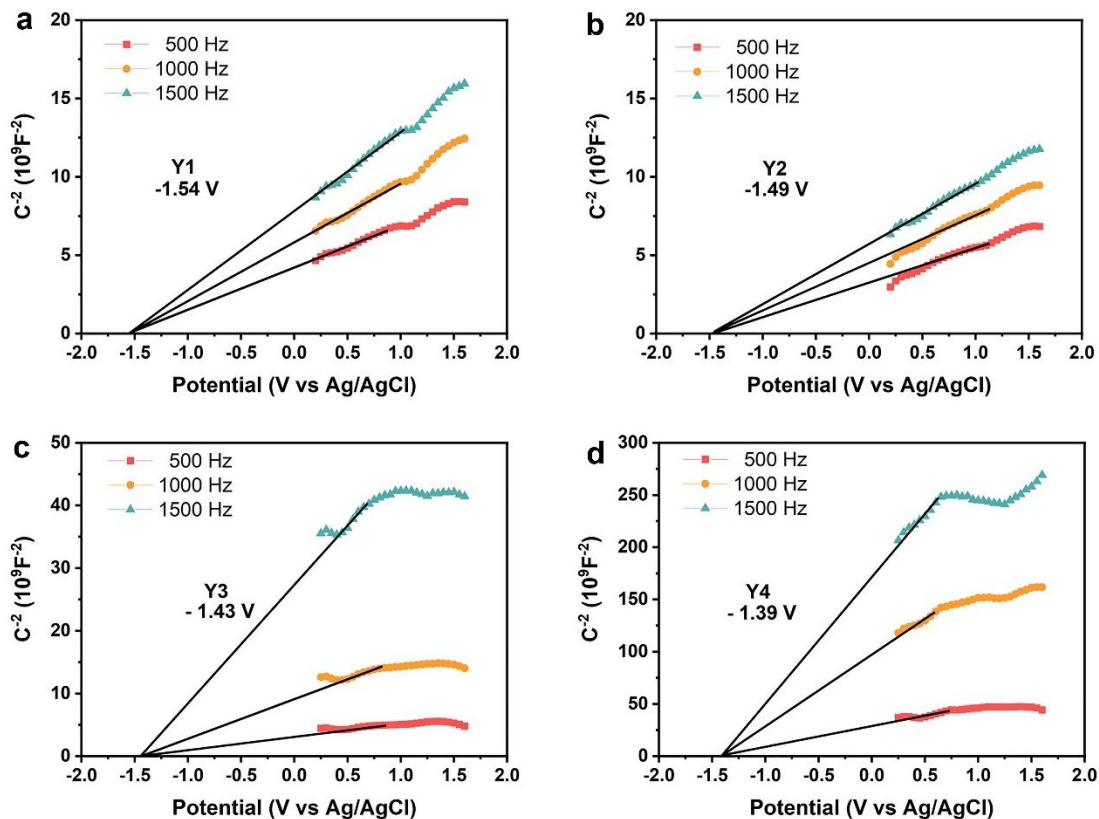


Fig. S6 The determined flat-band potential of (a) **Y1**, (b) **Y2**, (c) **Y3**, and (d) **Y4** by the Mott-Schottky method.

4. PHE Performance

4.1. HER Rates at The Initial Condition

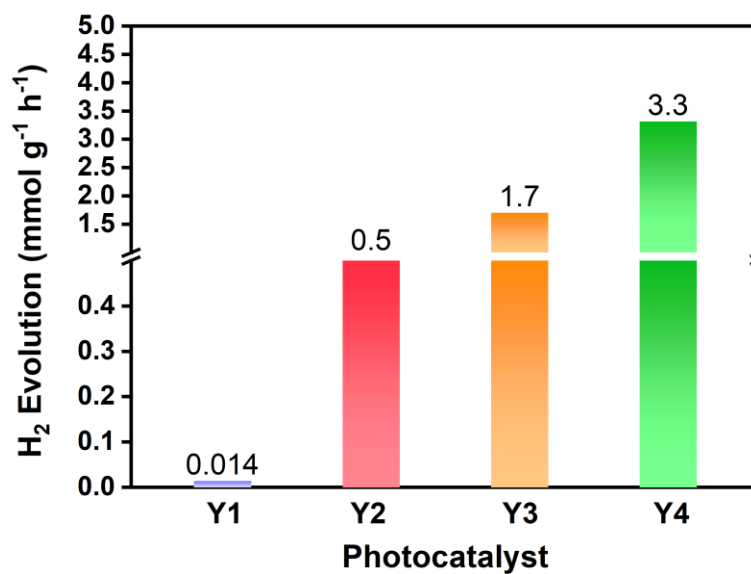


Fig. S7 HER rates at the initial condition. Catalyst 10 mg, H₂O 30 mL, AA 1 M, under visible light ($\lambda > 420$ nm).

4.2. Optimization of Co-solvents

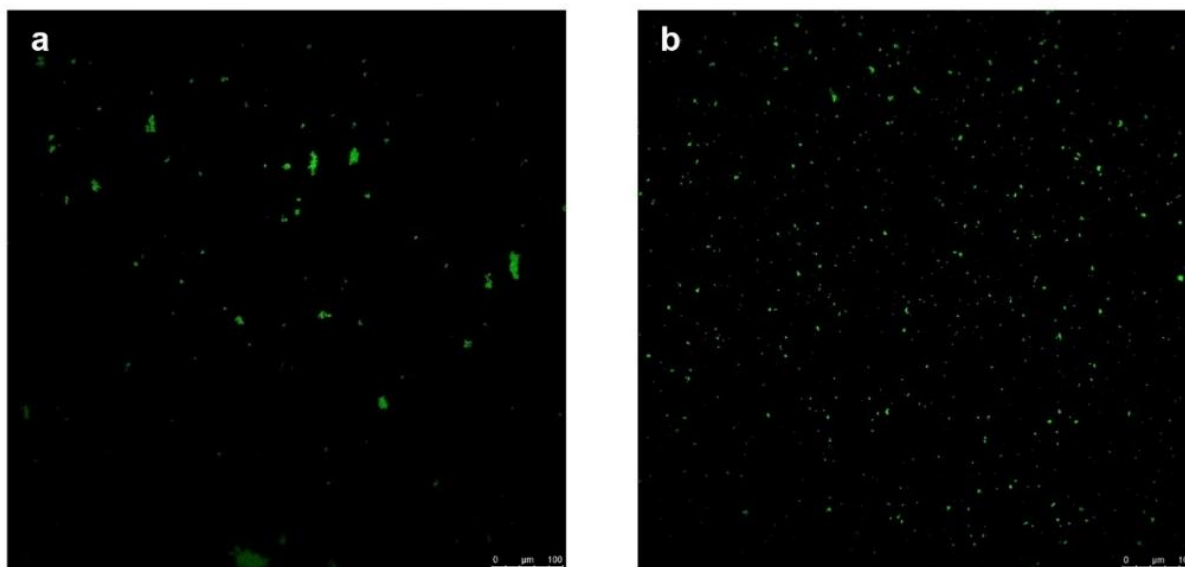


Fig. S8 CLSM spectra of Y4. Dispersion in (a) H₂O and (b) NMP.

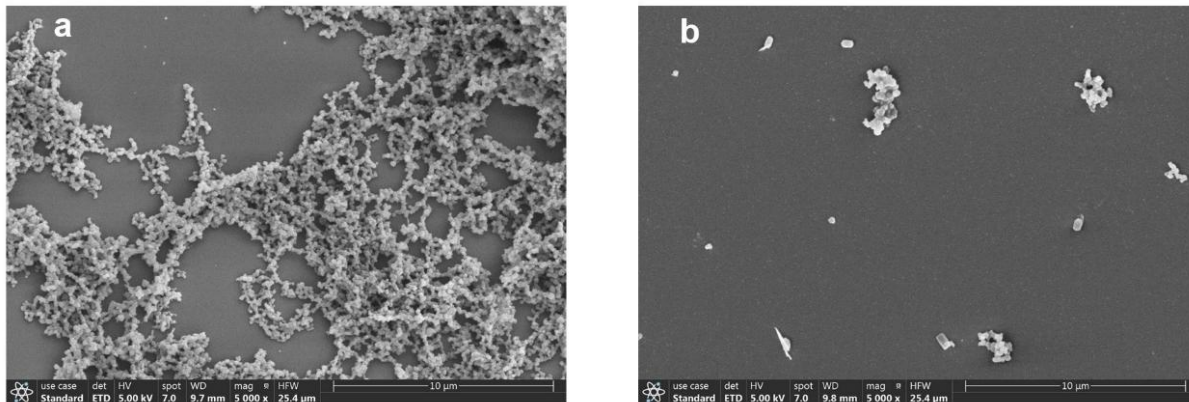


Fig. S9 SEM spectra of **Y4**. Dispersion in (a) H_2O and (b) NMP.

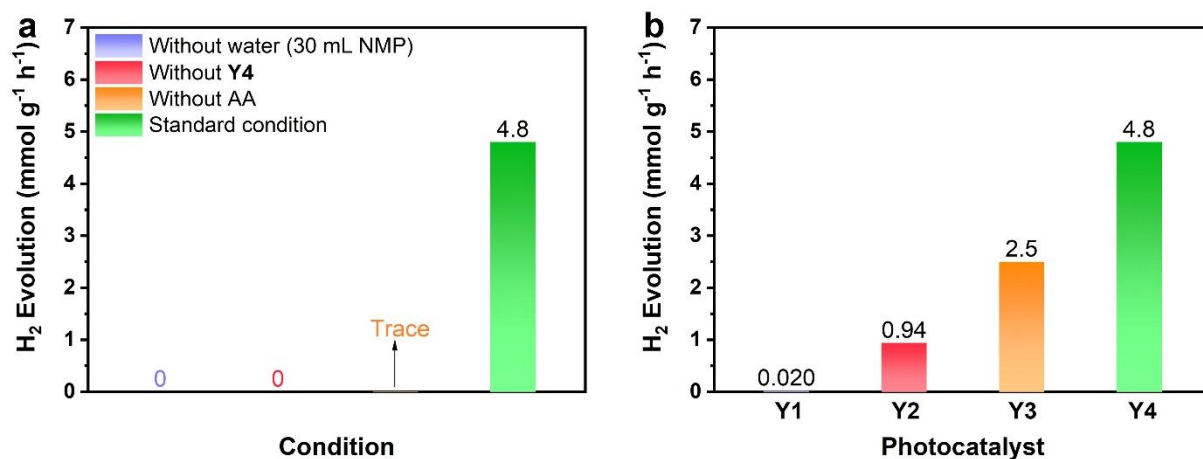


Fig. S10 (a) Demonstration that water is the only source of proton for PHE. (b) HER rates of four polymers ($\lambda > 420$ nm). Catalyst 10 mg, H_2O 27 mL, NMP 3 mL, AA 1 M.

4.3. Optimization of pH Values

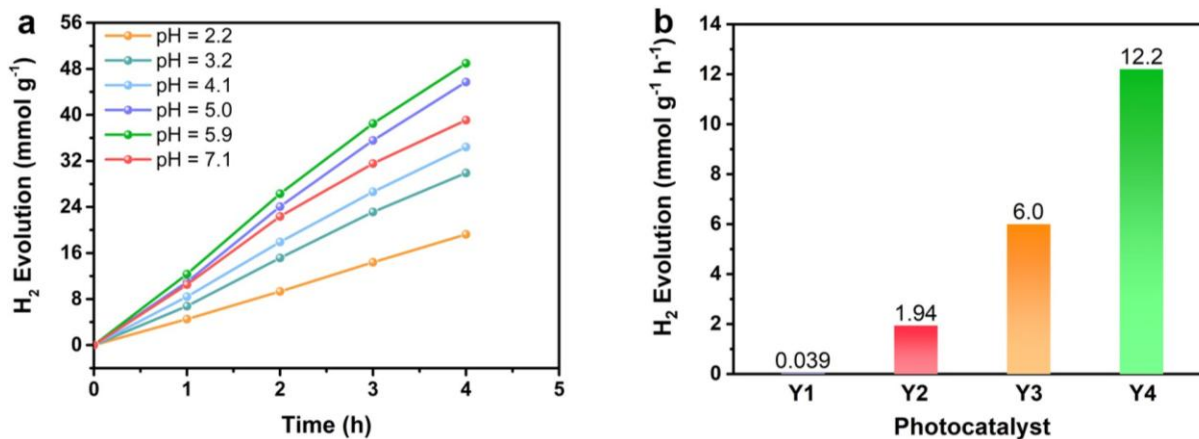


Fig. S11 Influence of pH values on the HER rates ($\lambda > 420$ nm). (a) **Y4** 10 mg, H₂O 27 mL, NMP 3 mL, AA 1 M, pH = x (x = 2.2, 3.2, 4.1, 5.0, 5.9, 7.1), pH values were adjusted by NaOH(s); (b) Catalyst 10 mg, H₂O 27 mL, NMP 3 mL, AA 1 M, pH = 5.9.

4.4. Optimization of Wavelength of Light

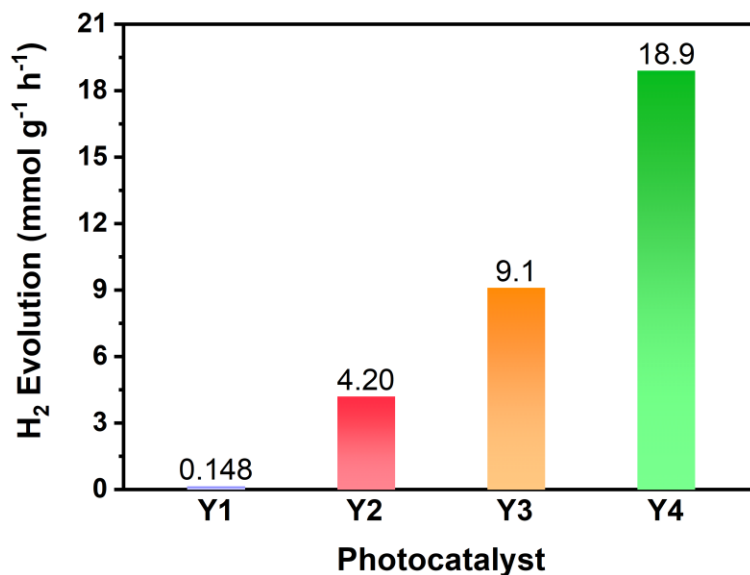


Fig. S12 HER rates of all polymers. Catalyst 10 mg, H₂O 27 mL, NMP 3 mL, AA 1 M, pH = 5.9 under UV-vis light ($\lambda > 300$ nm).

4.5. Optimization of Quantity of Photocatalysts

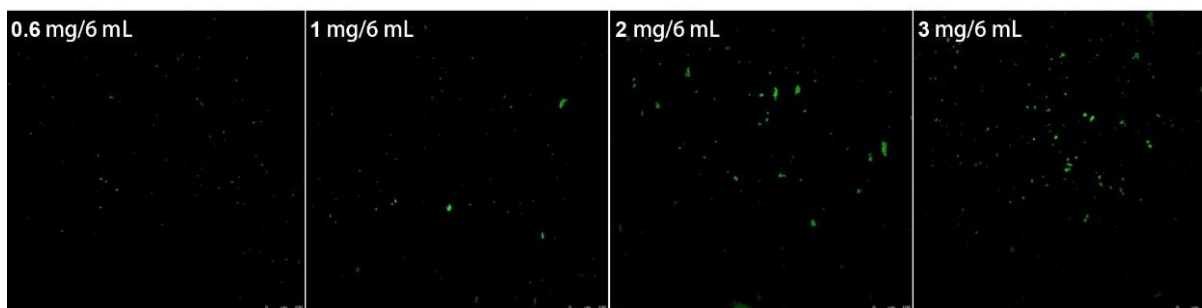


Fig. S13 CLSM spectra of Y4 with different quantities in 6 mL solvents.

4.6. In Comparison with g-C₃N₄

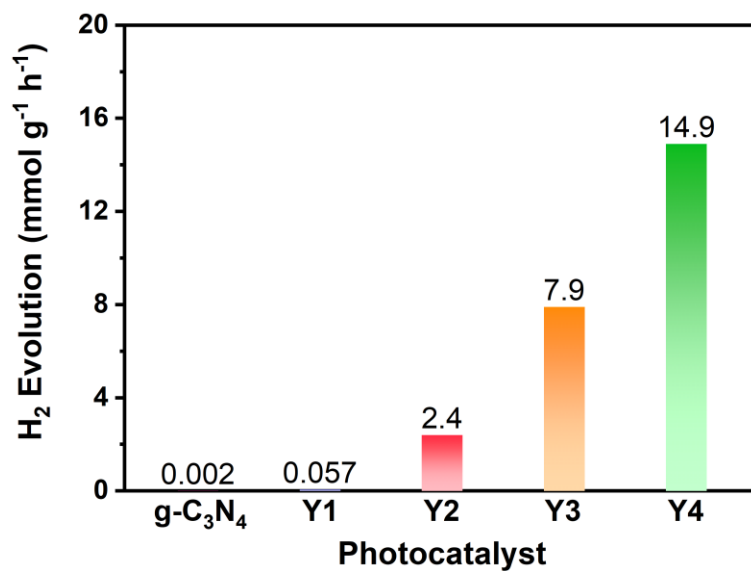


Fig. S14 HER rates in comparison with g-C₃N₄ ($\lambda > 420$ nm). Catalyst 5 mg, H₂O 27 mL, NMP 3 mL, AA 1 M, pH = 5.9.

4.7. Brief Summary on The Properties of All Polymers

Table S1 Brief summary on the properties of all polymers

Polymers	Optical gap (V)	S _{BET} (m ² /g)	HER ^a	HER ^b	HER ^c	HER ^d	HER ^e	HER ^f	AQY ^g (%)
Y1	2.86	553.0	0.014	0.020	0.039	0.148	0.057	0.470	-
Y2	2.59	549.8	0.53	0.94	1.94	4.20	2.40	5.77	-
Y3	2.47	495.7	1.7	2.5	6.0	9.1	7.9	14.4	-
Y4	2.42	328.2	3.3	4.8	12.2	18.9	14.9	27.0	8.5

All PHE performances were measured without any cocatalyst. ^{a, b, c, d, e, f} mmol g⁻¹ h⁻¹; ^a Catalyst 10 mg, H₂O 30 mL, AA 1 M under visible light ($\lambda > 420$ nm); ^b Catalyst 10 mg, NMP 3 mL, H₂O 27 mL, AA 1 M under visible light; ^c Catalyst 10 mg, NMP 3 mL, H₂O 27 mL, AA 1 M, pH = 5.9 under visible light, pH value was adjusted by NaOH(s); ^d Catalyst 10 mg, NMP 3 mL, H₂O 27 mL, AA 1 M, pH = 5.9, under UV-vis light ($\lambda > 300$ nm); Catalyst 5 mg, NMP 3 mL, H₂O 27 mL, AA 1 M, pH = 5.9 ^e under visible light and ^f under UV-vis light; ^g AQY = 8.5% was obtained at 420 nm.

4.8. Repeatability and Cycling Stability of Y4

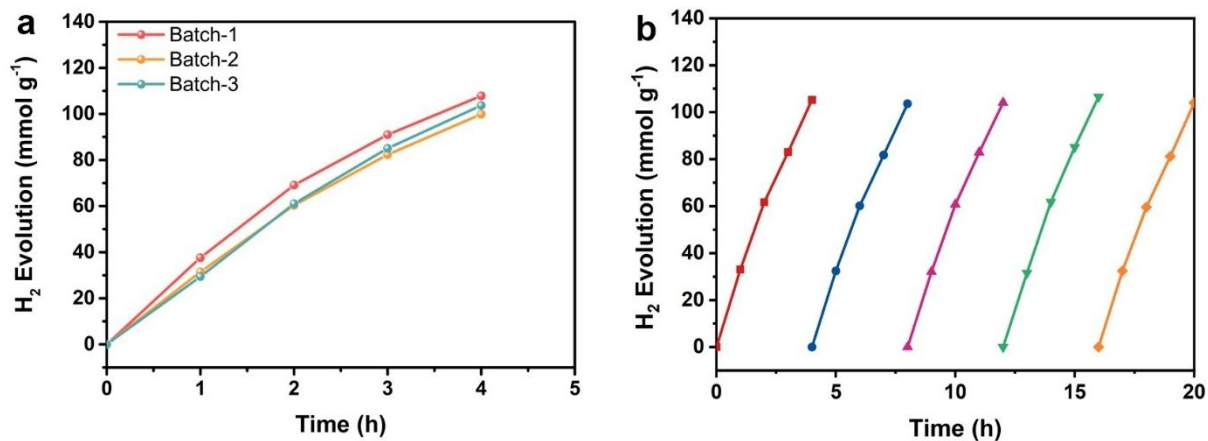


Fig. S15 (a) Repeatability and (b) cycling stability of Y4.

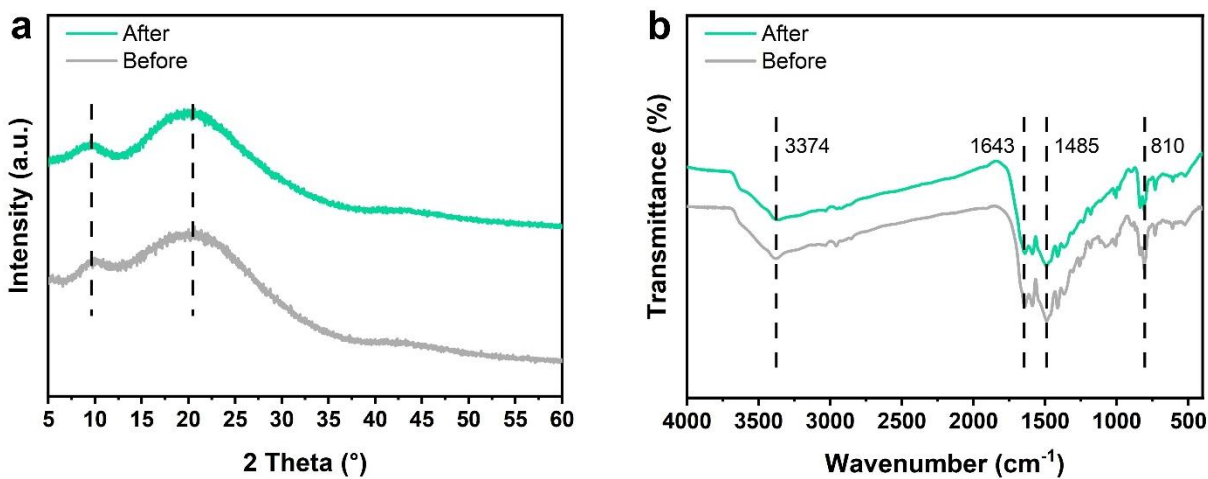


Fig. S16 XRD and FT-IR spectra of Y4 before and after the cycling experiment.

5. Summary of Recently Reported Literatures of PHE without Cocatalyst.

Table S2 Summary of recently reported literatures of PHE without cocatalyst

Photocatalysts	HERs (mmol g ⁻¹ h ⁻¹)	AQY (%)	References
Y4	27	8.5 (10 mg@420 nm)	This work
P7	5.8	7.2 (25 mg@420 nm)	<i>Angew. Chem. Int. Ed.</i> 2016 , 55, 1792. <i>Angew. Chem. Int. Ed.</i> 2018 , 57, 2520.
TATR-PPN	7.2	6.6 (5 mg@420 nm)	<i>Angew. Chem. Int. Ed.</i> 2024 , 63, e202319395.
P-TAME	10	8.9 (10 mg@420 nm)	<i>Angew. Chem. Int. Ed.</i> 2023 , 62, e202304875
FSO-FS	3.4	6.8 (50 mg@420 nm)	<i>Angew. Chem. Int. Ed.</i> 2019 , 58, 10236-10240.
P10	3.3	11.6 (25 mg@420 nm)	<i>Nat. Commun.</i> 2018 , 9, 4968.
B-FOBT-1,4-E	13.3	5.7 (30 mg@420 nm)	<i>ACS Energy Lett.</i> 2018 , 3, 2544.
ZnCoP-F CP	2.76	6.92 (30 mg@400 nm)	<i>Adv. Funct. Mater.</i> 2021 , 31, 2009819.
PCP4e	9.34	0.34 (3.5 mg@420 nm)	<i>J. Am. Chem. Soc.</i> 2016 , 138, 7681-7686.
PIFDTBT	0.58	3.4 (20 mg@420 nm)	<i>Appl. Catal. B</i> 2019 , 259, 118067.
CP-St	143	9.6 (12 mg@550 nm)	<i>J. Mater. Chem. A</i> 2020 , 8, 5890-5899.
PySO	11.2	3.25 (10 mg@420 nm)	<i>Small</i> 2018 , 14, 1801839.
P28	1.34	6.7 (25 mg@420 nm)	<i>Chem. Mater.</i> 2018 , 30, 5733-5742.
S-CMP3	11.2	13.2 (30 mg@420 nm)	<i>Chem. Mater.</i> 2019 , 31, 305-313.
P12	10.5	1.4 (25 mg@420 nm)	<i>J. Mater. Chem. A</i> 2018 , 6, 11994-12003.
PyDF	4.09	4.5 (15 mg@420 nm)	<i>Green Chem.</i> 2018 , 20, 664.
F _{0.5} CMP	1.76	5.8 (5 mg@400 nm)	<i>Chem. Eur. J.</i> 2019 , 25, 3867-3874
PyTh-CPP	16.69	6.24 (30 mg@420 nm)	<i>Chem. Eng. J.</i> 2022, 446 , 137158.
BTT-CPP	37.87	3.30 (6 mg@365 nm)	<i>Macromolecules</i> 2021 , 54, 2661-2666.
PF6A-SF	36.43	2.95 (5 mg@405 nm)	<i>Polymer</i> 2022 , 240, 124509.
Py-ThTh-CMP	1.87	3.4 (3 mg@420 nm)	<i>J. Colloid Interface Sci.</i> 2023 , 637, 41-54.
N-PDBT-O	12.2	3.7 (30 mg@420 nm)	<i>Macromol. Rapid Commun.</i> 2019 , 40, 1800494.
PyDTDO-3	24.97	3.93 (10 mg@550 nm)	<i>Chem. Sci.</i> 2021 , 12, 1796-1802.

6. Dynamics Behaviours of Photoexcited Carriers

6.1. EPR and Contact Angle Measurements

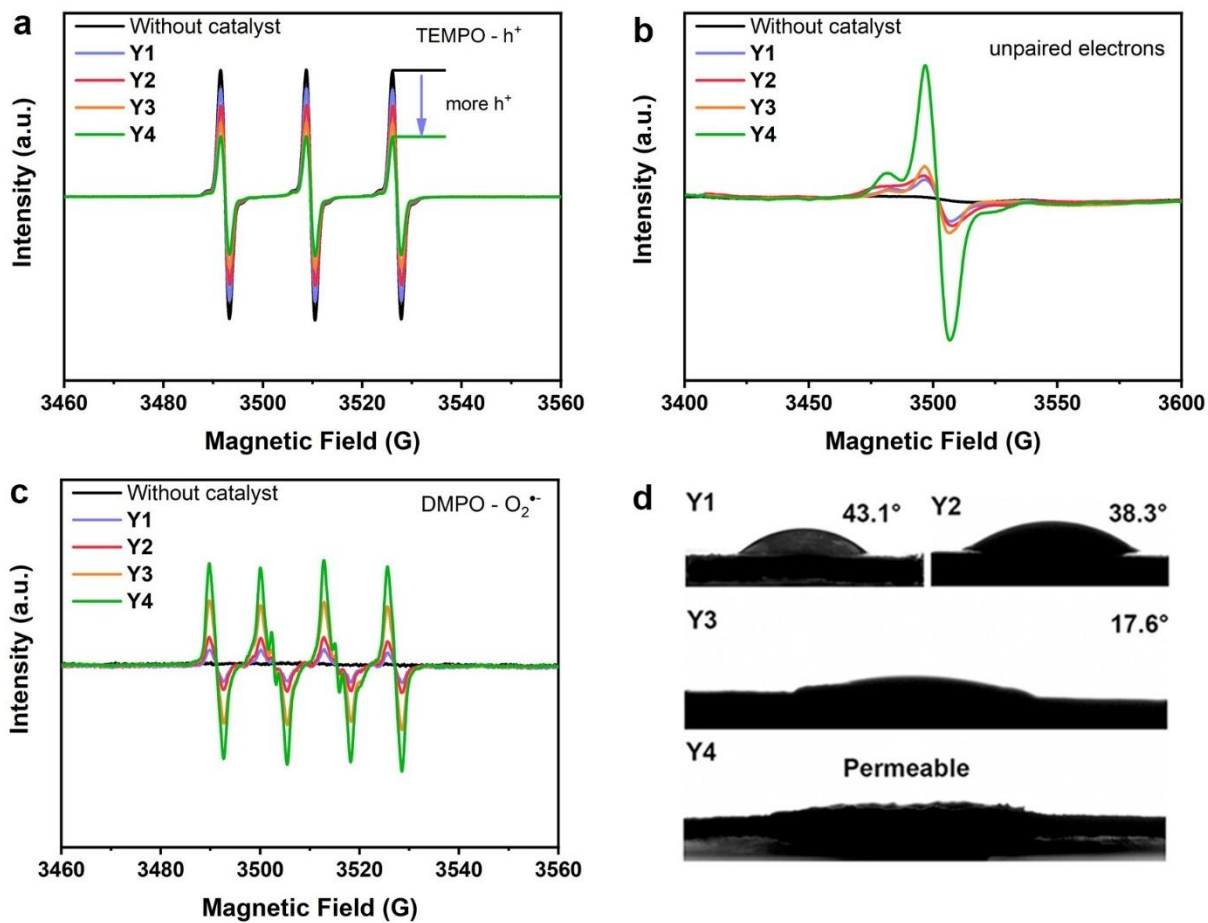


Fig. S17 EPR signals of all polymers, (a) hole trapped by TEMPO, (b) unpaired electrons, and (c) O_2^- trapped by DMPO; (d) contact angle between CMPs and H_2O .

6.2. Temperature-dependent Photoluminescence

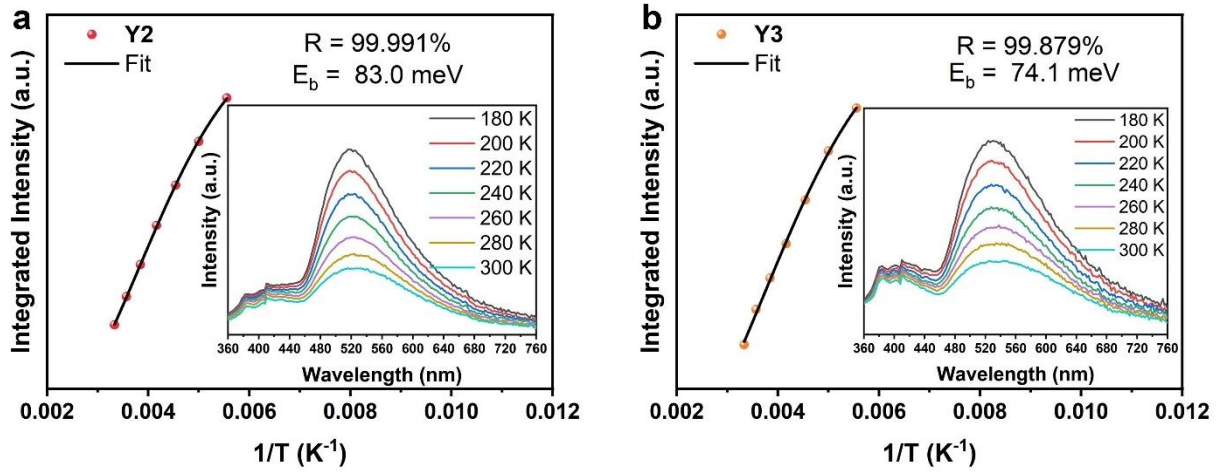


Fig. S18 Temperature-dependent photoluminescence spectra of (a) **Y2** and (b) **Y3** from 180 to 300 K ($\lambda_{ex} = 330$ nm).

6.3. Fs-TA Measurements

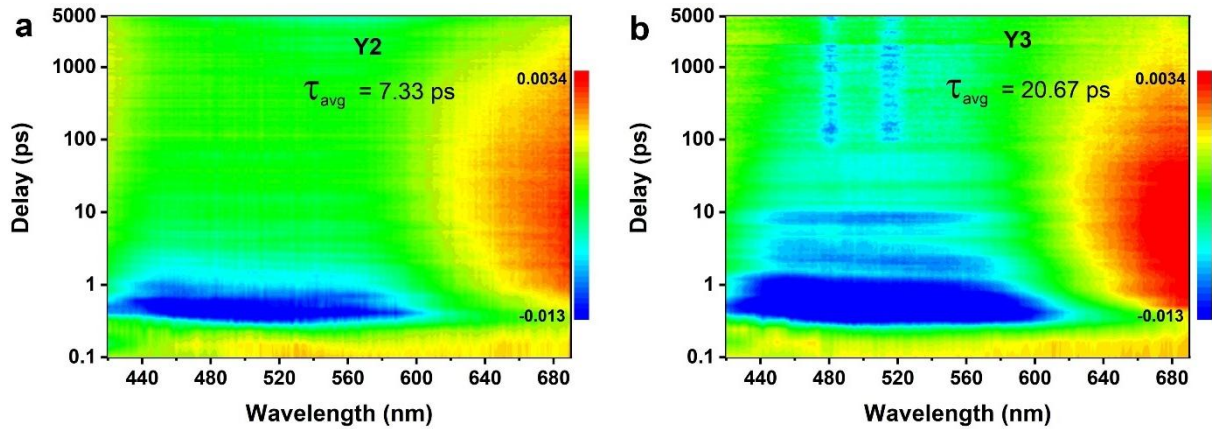


Fig. S19 Fs-TA spectra of (a) **Y2** and (b) **Y3** ($\lambda_{ex} = 360$ nm).

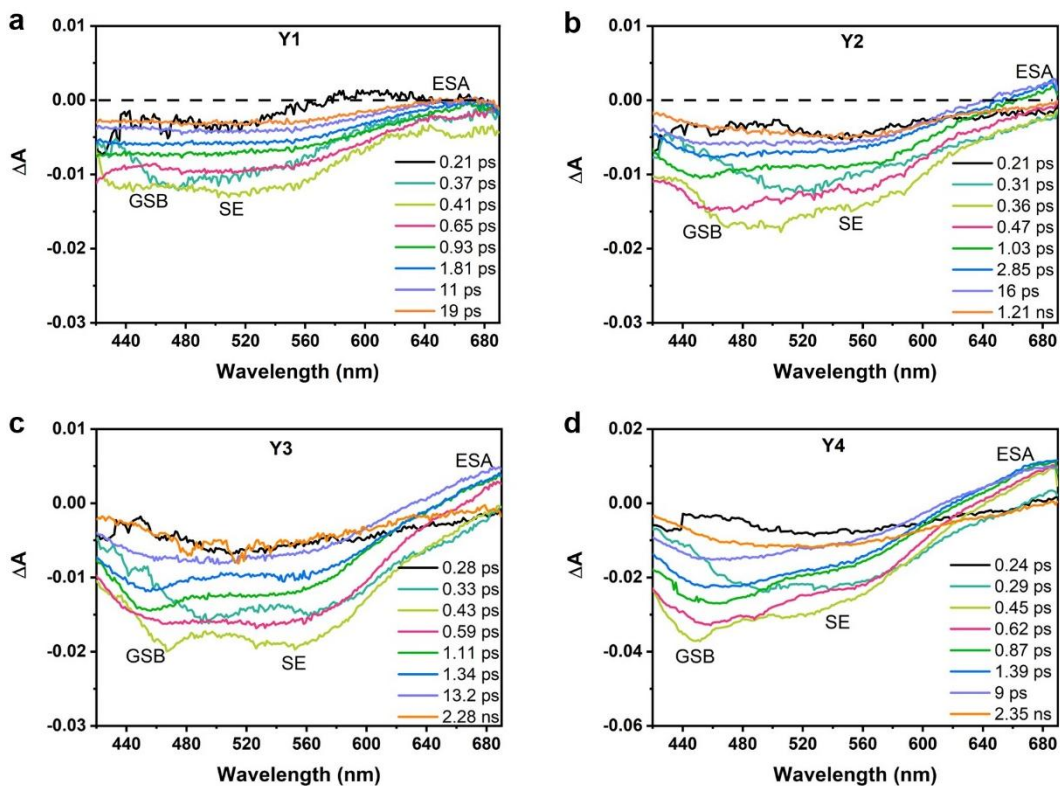


Fig. S20 The TA spectra with fs-ns timescales of (a) **Y1**, (b) **Y2**, (c) **Y3** and (d) **Y4**.

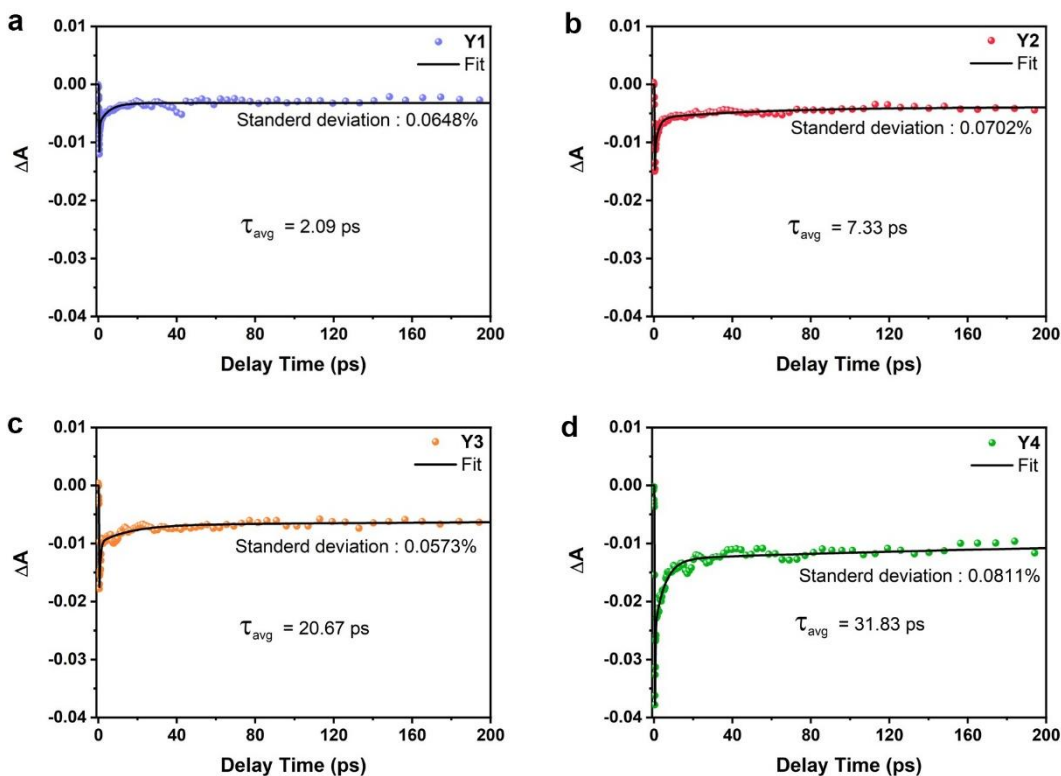


Fig. S21 Fs-TA decay kinetic curves of (a) **Y1**, (b) **Y2**, (c) **Y3** and (d) **Y4**.

7. Theoretical Calculations

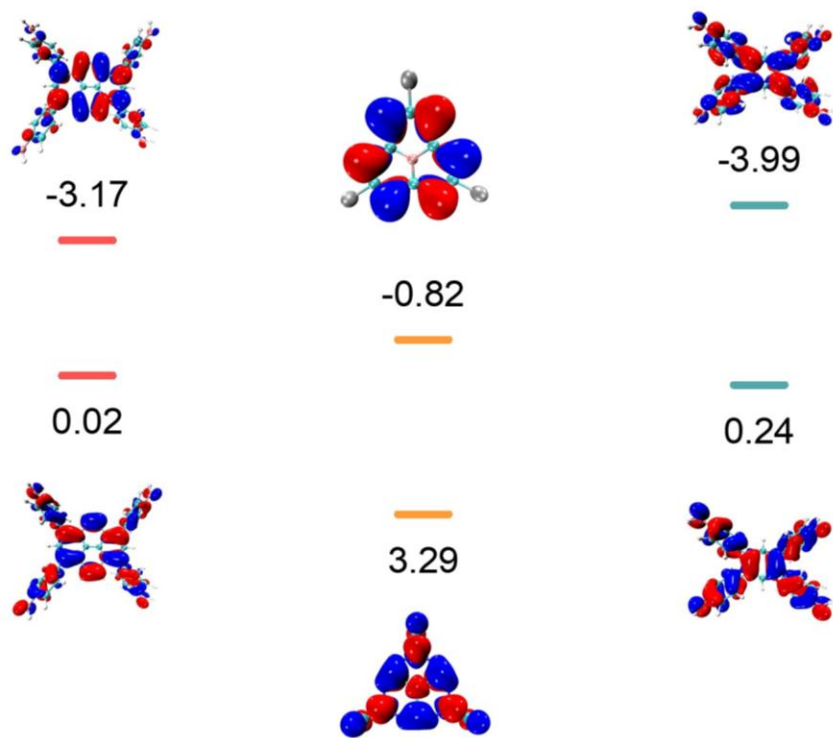


Fig. S22 Frontier molecular orbital diagrams of TAPPy, Cy and TAPB.

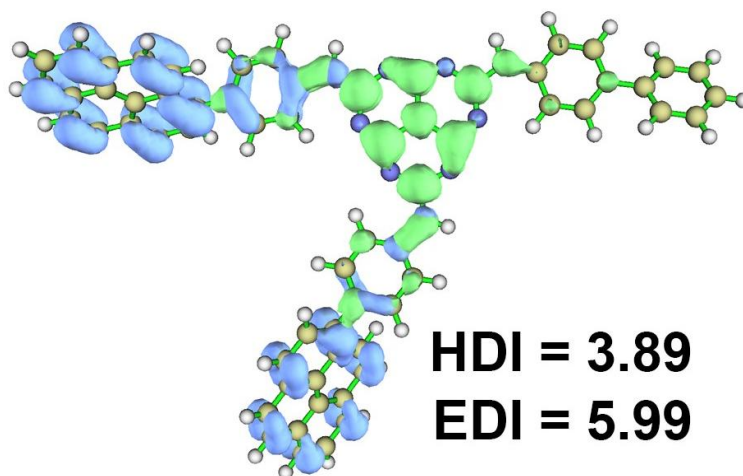


Fig. S23 Real-space hole (blue regions) and electron (green regions) distributions in the model structure in **Y3** (isovalue = 0.0007).

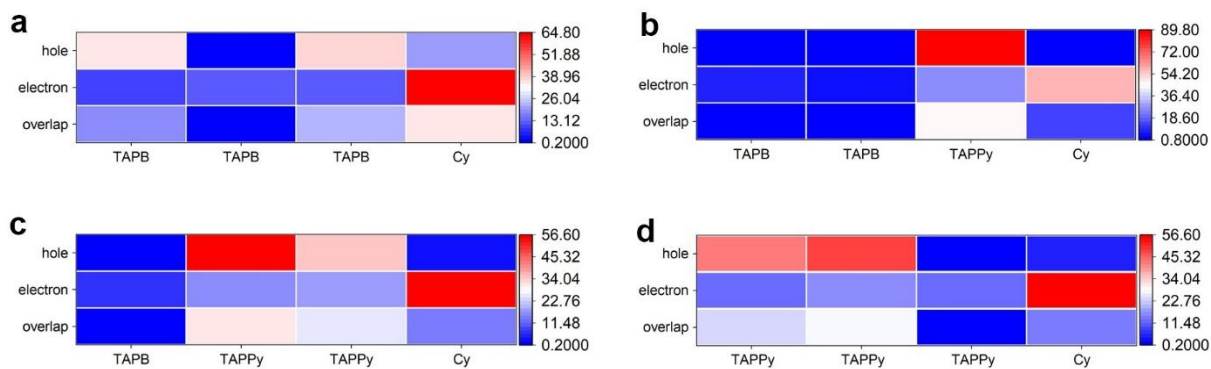


Fig. S24 Heat maps of all model structures in (a) Y1, (b) Y2, (c) Y3 and (d) Y4.

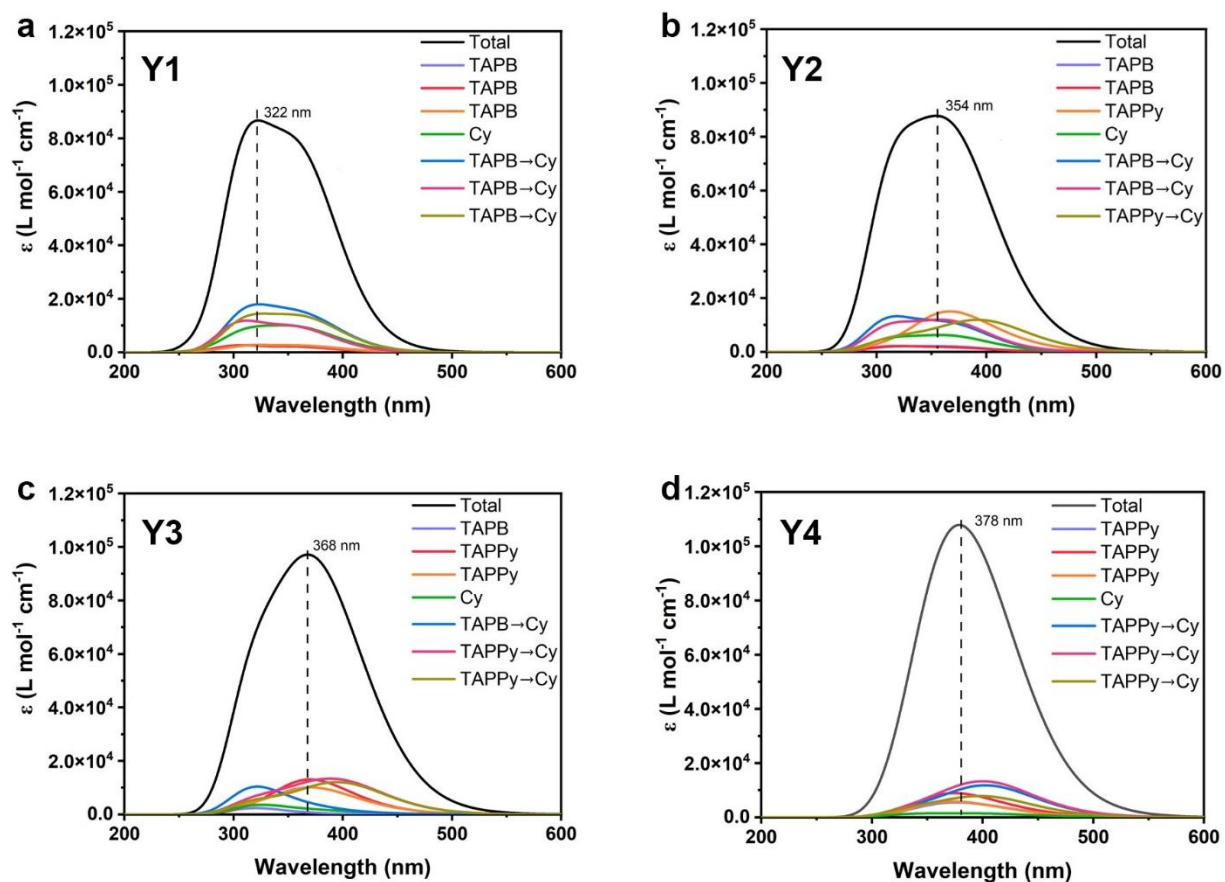


Fig. S25 The CTS of the model structures in (a) Y1, (b) Y2, (c) Y3 and (d) Y4.

Table S3 The calculated S1 of model structures of all CMPs.

Item	Transition from HOMO to LUMO	f
Y1	90.5%	0.97
Y2	96.2%	0.45
Y3	80.4%	0.41
Y4	85.3%	0.85

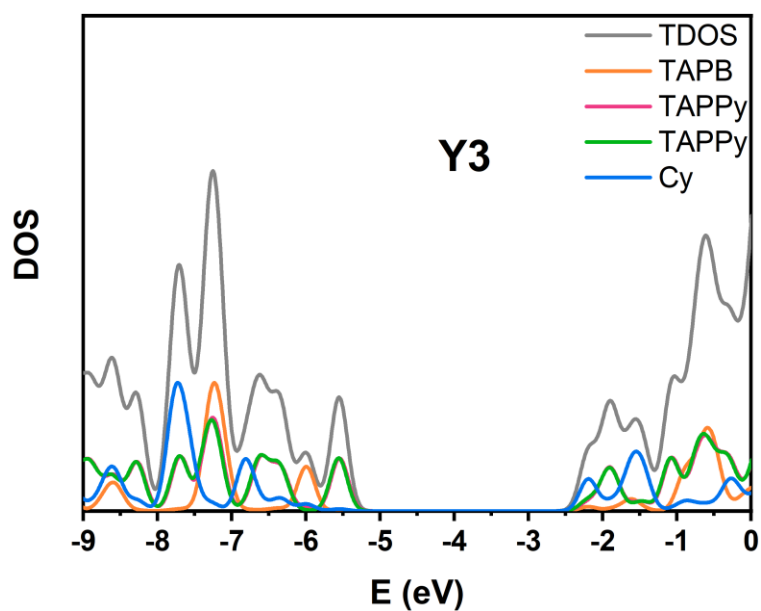


Fig. S26 The DOS spectrum of model structure in Y3.

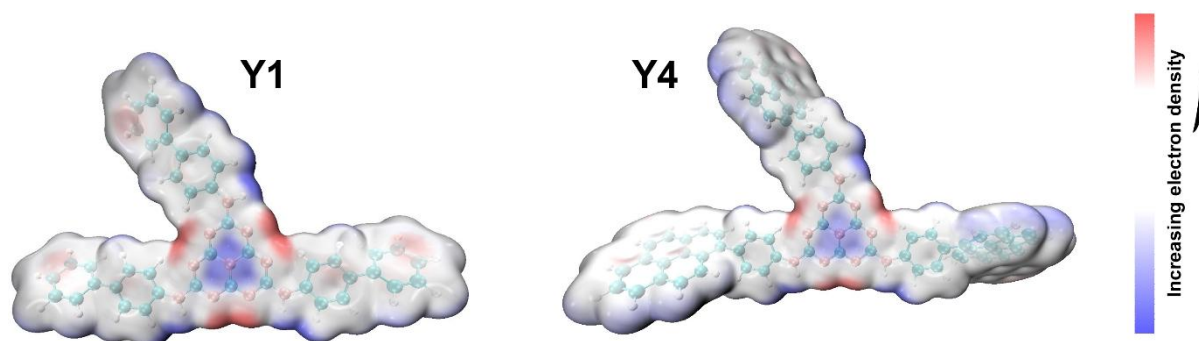


Fig. S27 The surface electrostatic distribution spectra of model structures in Y1 and Y4.

8. NMR Spectra

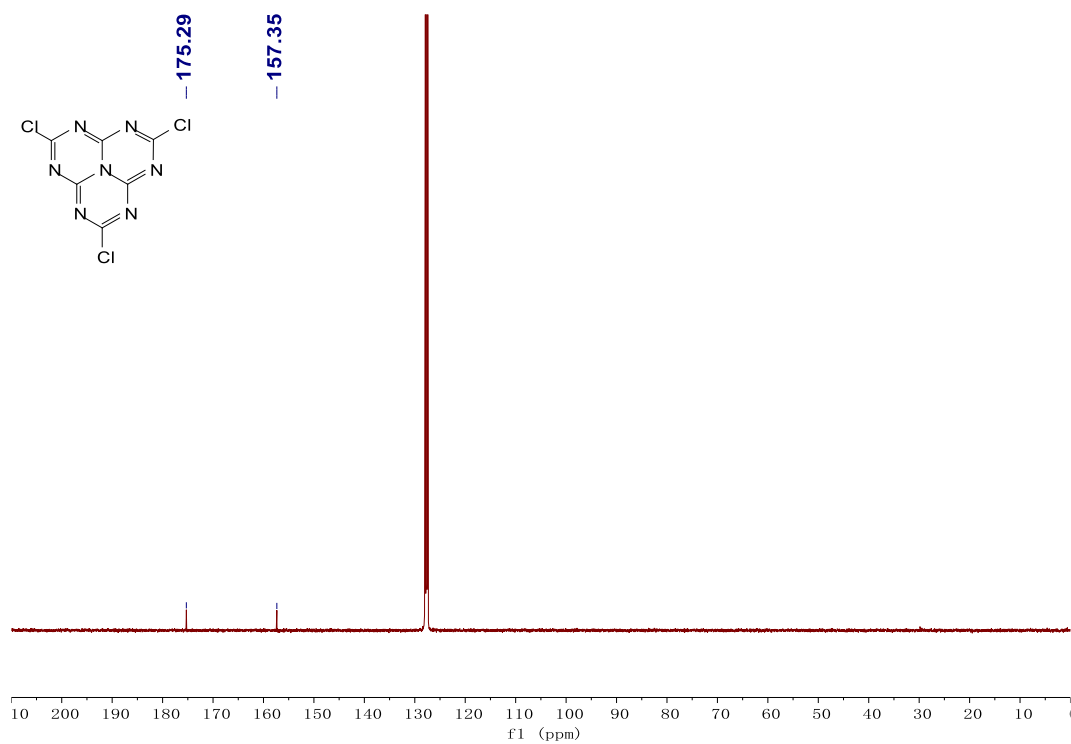


Fig. S28 ¹³C NMR spectrum of Cy.

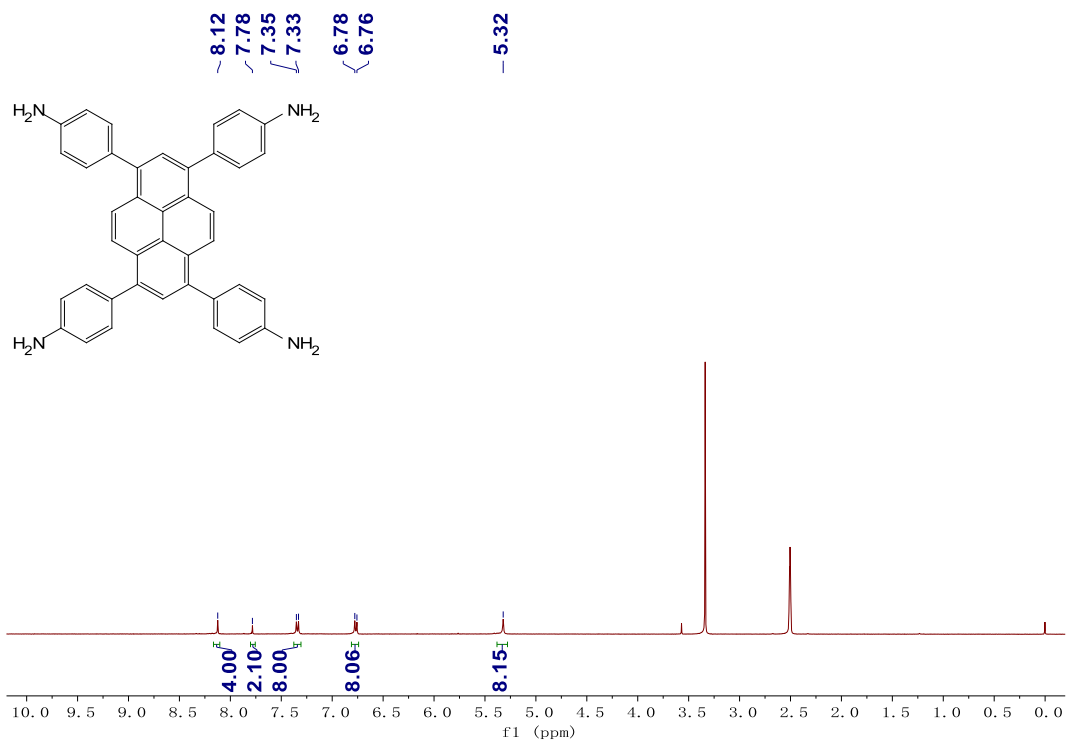


Fig. S29 ¹H NMR spectrum of TAPPy.

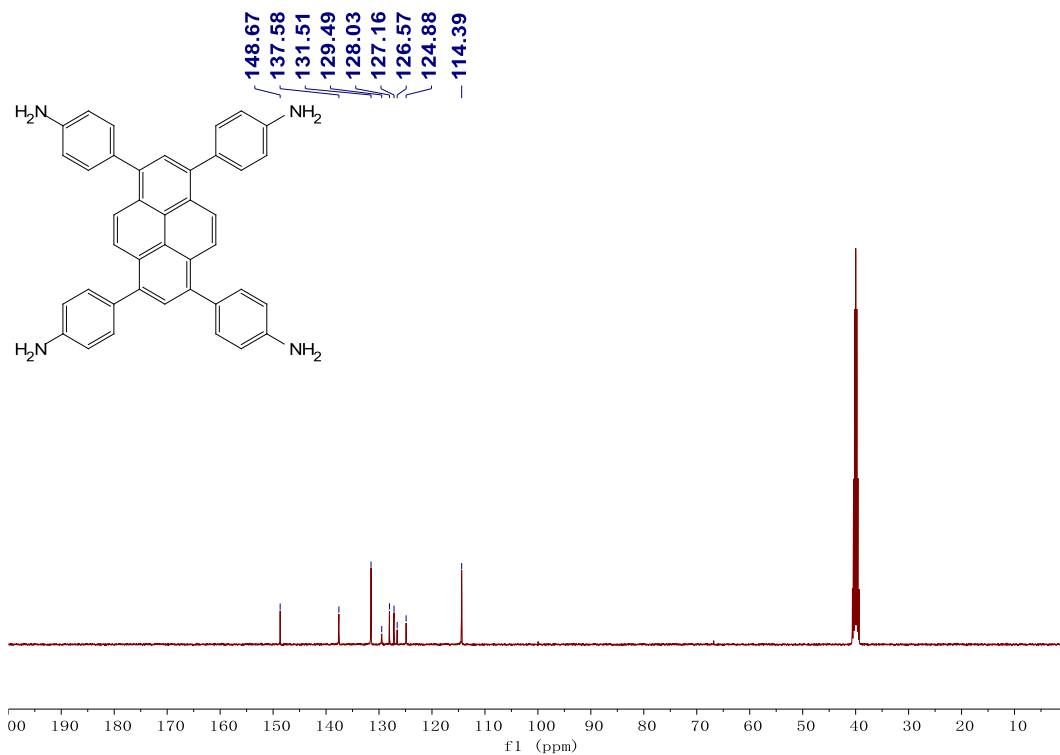


Fig. S30 ^{13}C NMR spectrum of TAPPY.

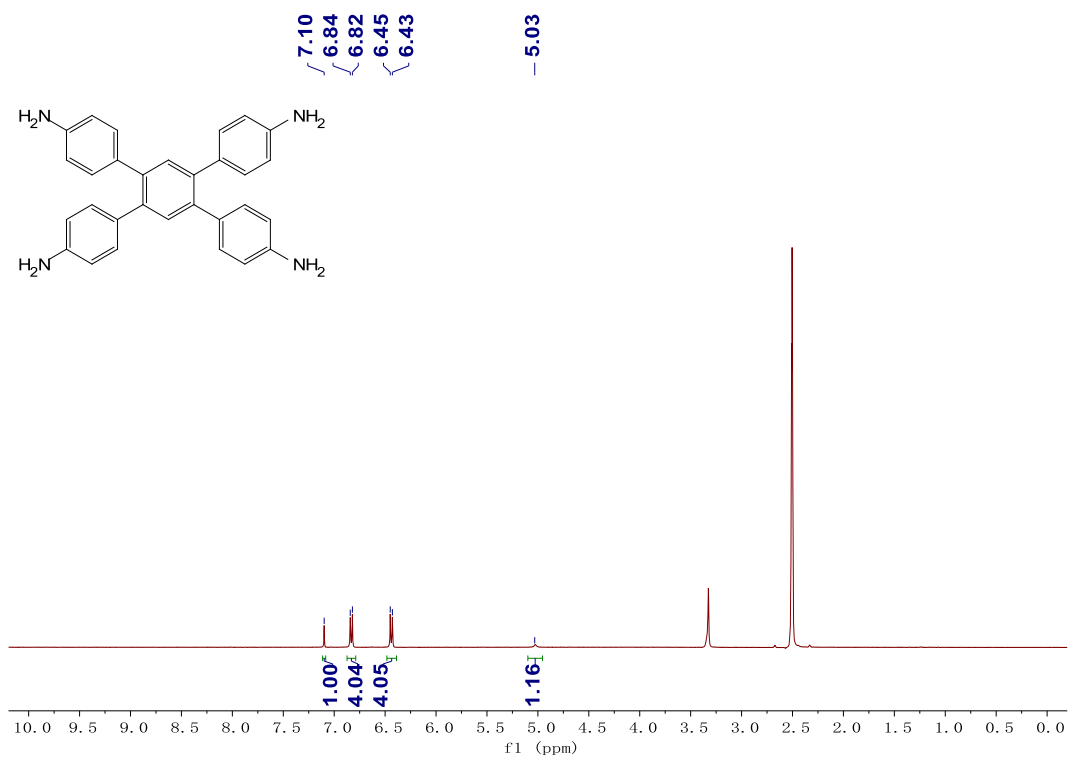


Fig. S31 ^1H NMR spectrum of TAPB.

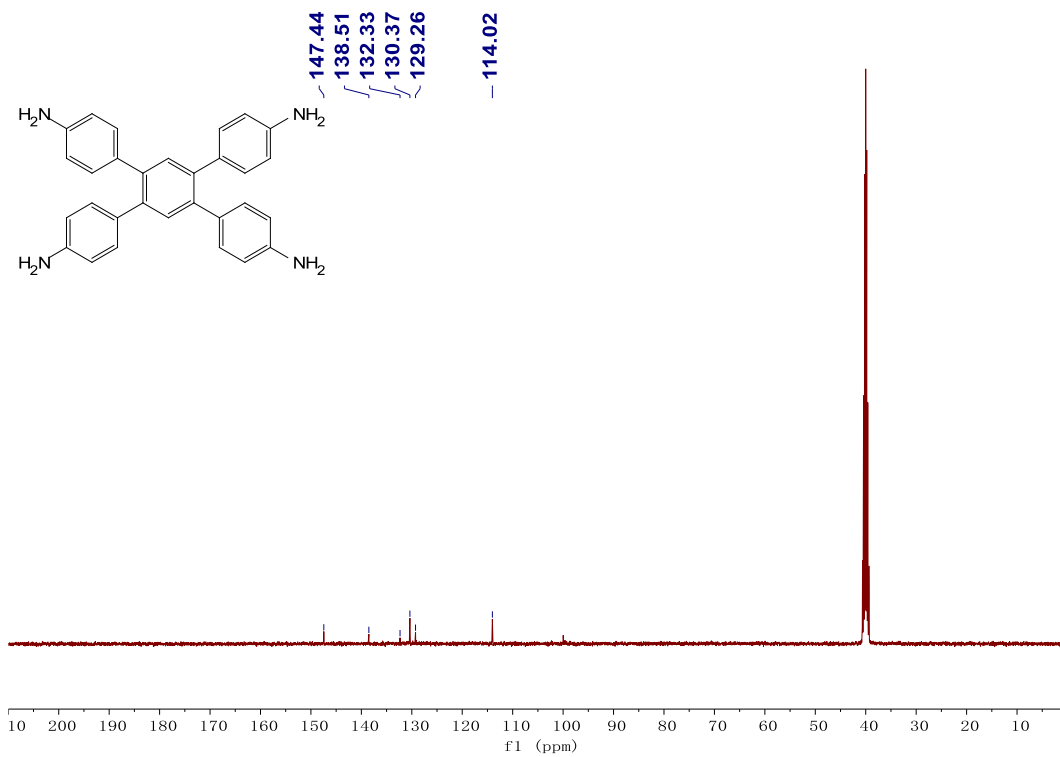


Fig. S32 ¹³C NMR spectrum of TAPB.

References

1. J.-Z. Cheng, L.-L. Liu, G. Liao, Z.-Q. Shen, Z.-R. Tan, Y.-Q. Xing, X.-X. Li, K. Yang, L. Chen and S.-Y. Liu, *J. Mater. Chem. A*, 2020, **8**, 5890-5899.
2. S. Ghosh, A. Nakada, M. A. Springer, T. Kawaguchi, K. Suzuki, H. Kaji, I. Baburin, A. Kuc, T. Heine, H. Suzuki, R. Abe and S. Seki, *J. Am. Chem. Soc.*, 2020, **142**, 9752-9762.
3. J. Kim, J. P. Jeon, Y. H. Kim, N. T. D. Anh, K. Chung, J. M. Seo and J. B. Baek, *Angew. Chem. Int. Ed.*, 2024, **63**, e202319395.
4. Z. A. Lan, G. Zhang, X. Chen, Y. Zhang, K. A. I. Zhang and X. Wang, *Angew. Chem. Int. Ed.*, 2019, **58**, 10236-10240.
5. Y. Liu, J. Wu and F. Wang, *Appl. Catal., B Environ.*, 2022, **307**, 121144.
6. Z. Luo, X. Chen, Y. Hu, X. Chen, W. Lin, X. Wu and X. Wang, *Angew. Chem. Int. Ed.*, 2023, **62**, e202304875.
7. C. Shu, C. Han, X. Yang, C. Zhang, Y. Chen, S. Ren, F. Wang, F. Huang and J. X. Jiang, *Adv. Mater.*, 2021, **33**, 2008498.
8. M. J. Frisch, **et al**, Gaussian 09, Gaussian Inc., Wallingford CT, 2009.
9. T. Lu and F. Chen, *J. Comput. Chem.*, 2011, **33**, 580-592.
10. X. Wang, K. Maeda, A. Thomas, K. Takanabe, G. Xin, J. M. Carlsson, K. Domen and M. Antonietti, *Nat. Mater.*, 2009, **8**, 76-80.
11. Z. Xie, W. Wang, X. Ke, X. Cai, X. Chen, S. Wang, W. Lin and X. Wang, *Appl. Catal., B Environ.*, 2023, **325**, 122312.
12. L. Ascherl, E. W. Evans, J. Gorman, S. Orsborne, D. Bessinger, T. Bein, R. H. Friend and F. Auras, *J. Am. Chem. Soc.*, 2019, **141**, 15693-15699.
13. H. L. Nguyen, C. Gropp, Y. Ma, C. Zhu and O. M. Yaghi, *J. Am. Chem. Soc.*, 2020, DOI: 10.1021/jacs.0c11064, 20335–20339.
14. S. Kumar, V. R. Battula, N. Sharma, S. Samanta, B. Rawat and K. Kailasam, *J. Mater. Chem. A*, 2022, **10**, 14568-14575.
15. V. R. Battula, S. Kumar, D. K. Chauhan, S. Samanta and K. Kailasam, *Appl. Catal., B Environ.*, 2019, **244**, 313-319.